

# A Nanosystem Alleviates Severe Acute Pancreatitis via Reactive Oxygen Species Scavenging and Enhancing Mitochondrial Autophagy

Liying Wang,<sup>†</sup> Zerui Gao,<sup>†</sup> Mengxiang Tian,<sup>†</sup> Li Liu, Jinyan Xie, Muxiong Chen, Zihao Huang, Bingzhi Dong, Weiqi Li, Liang Shi, Yifan Tong, Hongxia Xu, Bo Shen, Dong Cen,<sup>\*</sup> Hong Yu,<sup>\*</sup> and Xin Yu<sup>\*</sup>



Cite This: *Nano Lett.* 2025, 25, 8644–8654



Read Online

ACCESS |



Metrics & More



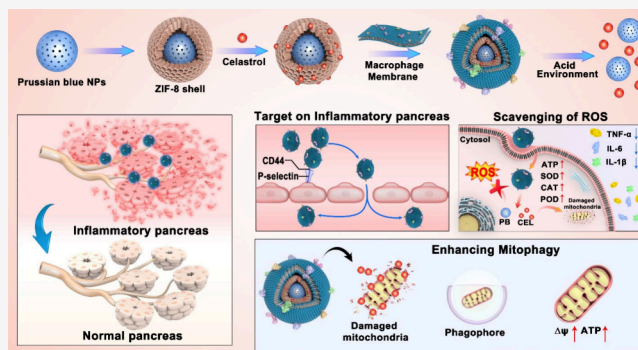
Article Recommendations



Supporting Information

**ABSTRACT:** Severe acute pancreatitis (SAP) is a life-threatening condition characterized by excessive reactive oxygen species (ROS) production and impaired mitochondrial function, resulting from disrupted autophagic flux. Current clinical treatment for SAP fails to address the condition comprehensively, with the treatment targeting only a single pathogenesis. Herein, we report an innovative acid-responsive biomimetic nanozyme. This system features a hollow Prussian blue (PB) core, serving as an ROS scavenger encapsulated within a porous ZIF-8 shell, enabling the efficient delivery of celastrol that activates autophagic flux. Encased in a macrophage membrane, this system selectively targets inflamed pancreatic tissues and is readily internalized by pancreatic acinar cells. This dual-scavenging mechanism effectively attenuates inflammatory cytokine levels and restores mitochondrial homeostasis in three distinct SAP mouse models. Overall, this study presents a promising synergistic strategy for the dual scavenging of damaged mitochondria and ROS, offering a novel therapeutic approach to the treatment of SAP.

**KEYWORDS:** severe acute pancreatitis, mitophagy, celastrol, biomimetic nanoparticle, combination therapy



Severe acute pancreatitis (SAP) is a life-threatening systemic inflammatory syndrome<sup>1,2</sup> with a mortality rate exceeding 30%.<sup>3</sup> Despite recent advancements in SAP treatment, the underlying mechanisms of cell damage and organ dysfunction remain unclear,<sup>4,5</sup> and the disease's complexity continues to pose significant treatment challenges. Clinically, SAP treatment relies heavily on broad-spectrum antibiotics, surgical debridement, and fluid resuscitation, which are insufficient to address the complex pathogenesis of this lethal condition. Therefore, developing novel therapeutic approaches targeting multiple pathways is essential.<sup>5</sup>

Among the various SAP pathologies, oxidative stress from excessive reactive oxygen species (ROS) generated by malfunctioning mitochondria plays a central role.<sup>4,6</sup> Necrotic pancreatic acinar cells trigger local inflammation and oxidative stress by releasing proinflammatory mediators and ROS,<sup>7</sup> leading to complex pathological processes, including systemic inflammatory response syndrome and multiple organ dysfunction syndrome.<sup>8</sup> Therefore, eliminating ROS is crucial in the treatment of SAP. ROS scavenging alone has shown preventive therapeutic effects in mild pancreatitis.<sup>9</sup> However, increased intercellular gaps between endothelial cells, leading to

enhanced vascular leakage in the pancreatic tissues of SAP, impair the permeability and diffusion of antioxidants.<sup>10,11</sup> High doses of antioxidant treatment are required to achieve efficient therapy for deadly SAP.<sup>12–14</sup> Recent studies have revealed that combining therapies to eliminate ROS is a promising approach for treating SAP.<sup>15,16</sup>

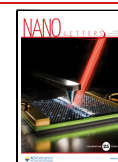
During SAP pathophysiology, autophagy of mitochondria, also called mitophagy, plays a key role in maintaining mitochondrial quality and quantity in pancreatic acinar cells.<sup>17</sup> By clearing damaged mitochondria, mitophagy prevents excessive inflammatory responses.<sup>18</sup> However, impaired autophagic flux during SAP disrupts mitophagy, leading to abnormal mitochondrial accumulation and worsening pancreatic necrosis and multiple organ dysfunction syndrome.<sup>19,20</sup> Recent studies have focused on reducing excess ROS to restore

**Received:** March 7, 2025

**Revised:** May 9, 2025

**Accepted:** May 9, 2025

**Published:** May 15, 2025



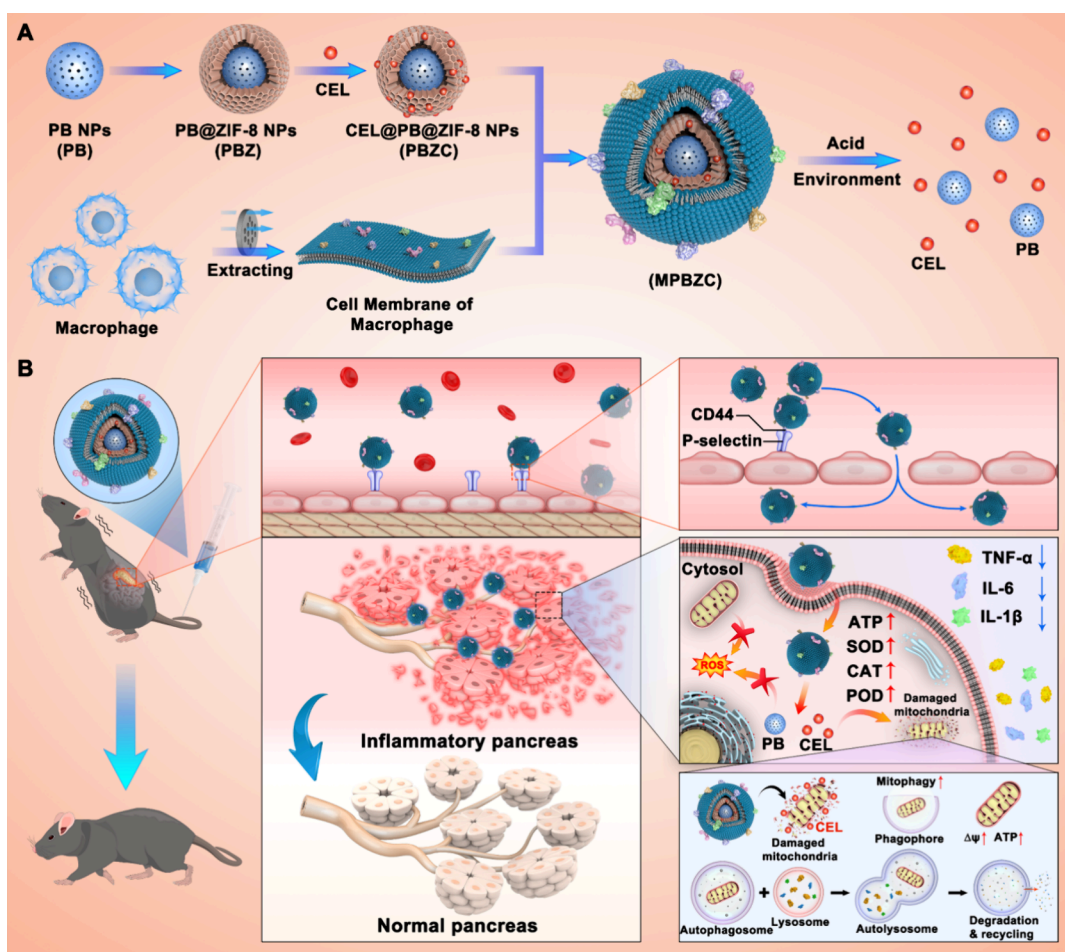


**Figure 1.** Synthesis, modification, and preparation of hierarchically porous a metal–organic framework biomimetic nanozyme and the synergistic strategy that dual-scavenged damaged mitochondria and ROS for the treatment of SAP. (A) Schematic diagram for the synthesis of MPBZC. The preparation of the acid-responsive hierarchically porous a metal–organic framework biomimetic nanozyme capable of carrying celastrol (CEL), extraction of macrophage membrane, and the preparation of MPBZC. The acidity-induced ZIF-8 degradation gradually released celastrol to promote mitophagy and the exposed PB core to reduce ROS. (B) Scheme targeting pancreatic tissue in an inflammatory state of pancreatitis and alleviating the SAP by restoring impaired autophagic flux and eliminating excessive ROS. Macrophage-membrane-coated core–shell-structured MPBZC binds to P-selectin highly expressed at the inflammatory site of SAP because of the interaction between chemokine receptors and adhesion molecules. This process provides specific targeting for MPBZC. The macrophage-membrane-coated MPBZC initiates endocytosis, allowing the core–shell structure MPBZC to enter the cells. The exposed PB core scavenges the cell's existing ROS, reduces serum amylase and inflammatory cytokine levels, and improves the antioxidant enzyme activity. Because autophagic flux was activated by celastrol loaded in MPBZC, mitophagy was improved and the mitochondrial membrane potential ( $\Delta\psi_m$ ) was recovered.

mitochondrial function, but this approach cannot eliminate damaged mitochondria.<sup>21–23</sup> Reducing ROS and restoring mitochondrial homeostasis are essential to improving SAP survival rates. However, no effective combination therapy currently exists to eliminate damaged mitochondria and ROS simultaneously in the treatment of SAP.

A natural compound from *Tripterygium wilfordii*, called celastrol (CEL), is widely studied for restoring autophagic flux.<sup>24</sup> However, its clinical application is hindered by poor water solubility and low oral absorption,<sup>25</sup> complicating its use in SAP treatment.<sup>26,27</sup> To overcome these issues, specialized drug-delivery systems, such as nanoparticles and liposomes, are required to enhance solubility and absorption efficiency. Macrophage-membrane-coated nanoparticles offer significant advantages over traditional delivery systems to accomplish combination therapy,<sup>28,29</sup> leading to long blood circulation and higher biocompatibility.<sup>30</sup> Biomimetic macrophage-membrane-coated nanocarriers specifically target the inflammatory environment of SAP through interactions between chemokine

receptors and adhesion molecules.<sup>31</sup> It is a promising strategy to deliver celastrol with biomimetic macrophage-membrane-coated nanocarriers in the combination therapy of SAP.

On the basis of these findings, we propose a combination strategy to simultaneously scavenge ROS and damaged mitochondria for treating SAP. Macrophage membranes are utilized to provide targeting capabilities and enhanced accumulation in the inflammation environment of SAP. Prussian blue (PB) serves as the core with outstanding ROS-scavenging capabilities, while the ZIF-8 agglomeration layer on its surface enables efficient celastrol loading. In acidic inflammatory microenvironments, ZIF-8 degradation releases celastrol to promote mitophagy, while the exposed PB core reduces ROS. The resulting macrophage-membrane-coated and ZIF-8-modified PB-nanoparticles-loaded celastrol (MPBZC) is readily taken up by acinar cells, demonstrating strong anti-inflammatory, antioxidant, and antiapoptotic effects. Additionally, by delivery of celastrol to acinar cells, MPBZC restores the autophagic flux inhibited during SAP. In

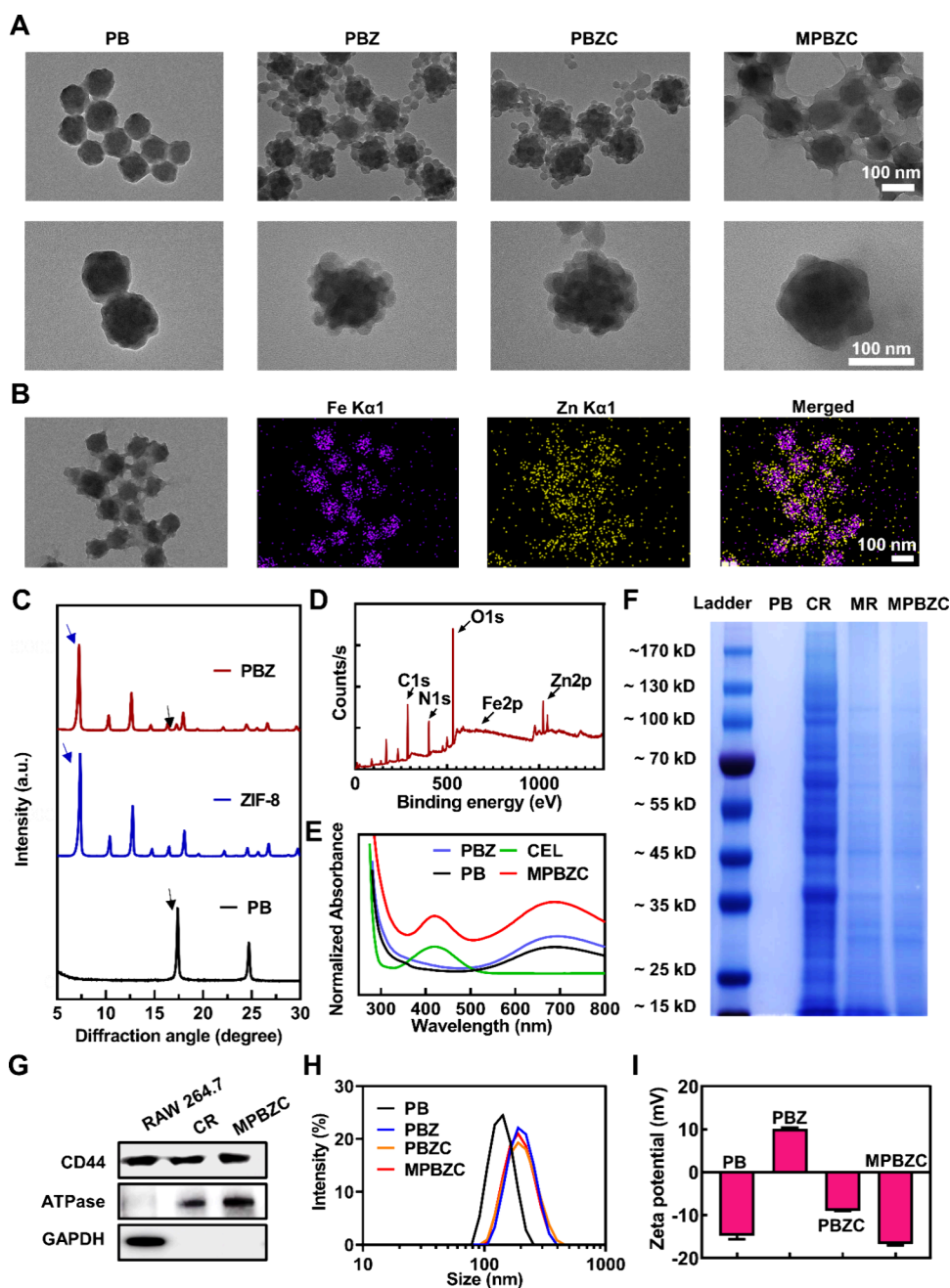
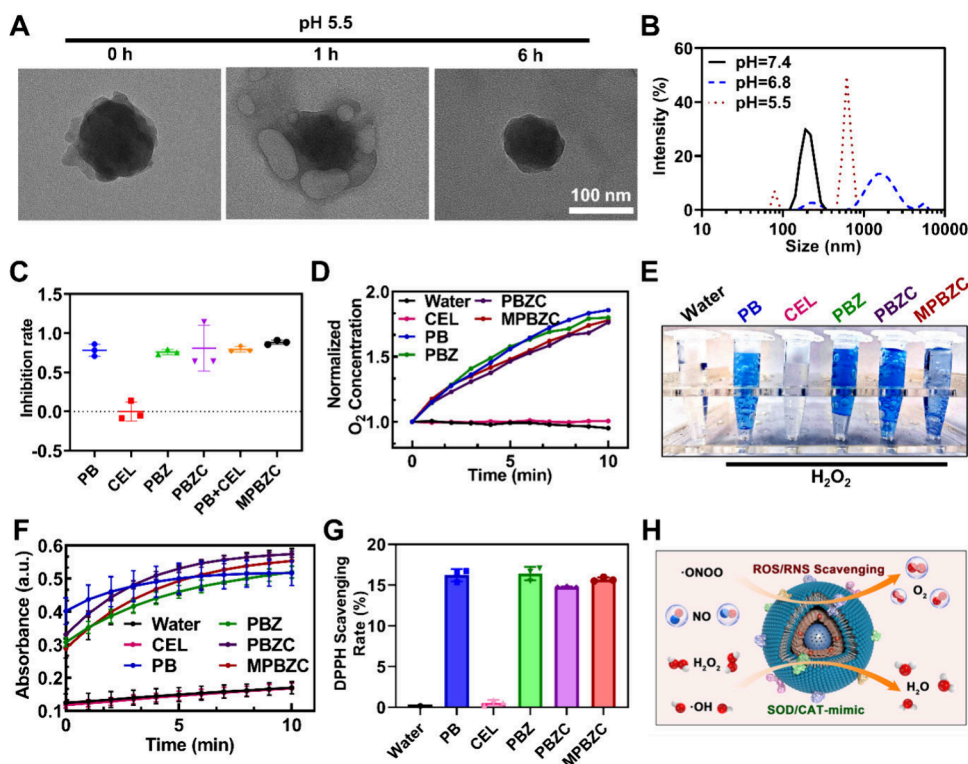


**Figure 2.** Characterization of MPBZC biomimetic nanoparticles. (A) TEM images of PB, PBZ, PBZC, and MPBZC (scale bar = 100 nm). (B) TEM-based elements (scale bar = 100 nm). (C) XRD patterns of PBZ, PB, and ZIF-8. (D) Full XPS of MPBZC. (E) UV-vis absorption spectra of PBZ, PB, CEL, and MPBZC. (F) Protein profiles of PB and CR (lysis solution of RAW264.7 cells), MR (lysis solution of a RAW264.7 membrane), and MPBZC. (G) Western blot analysis performed to detect the expression of CD44, ATPase, and GAPDH in RAW264.7, CR, and MPBZC. (H) Size distribution of PB, PBZ, PBZC, and MPBZC nanoparticles. (I)  $\zeta$  potential of PB, PBZ, PBZC, and MPBZC.

the SAP mouse model, MPBZC shows excellent pancreatic accumulation and retention, significantly reducing serum amylase, lipase, and inflammatory cytokine levels. Moreover, the dual strategy of scavenging ROS and damaged mitochondria increases the survival rate from 12.5% to 62.5% in a fatal SAP model. This well-designed MPBZC, through targeted drug delivery, not only eliminates excessive ROS but also restores autophagic flux, achieving a synergistic effect that markedly improves pancreatic tissue recovery and function. Thus, the proposed dual strategy of scavenging ROS and damaged mitochondria offers new insights and directions for treating life-threatening SAP.

The synthetic procedure employed to obtain the macrophage-membrane-coated MPBZC nanoparticles is outlined in Figure 1. First, PB nanoparticles were synthesized via a reported solvothermal reaction,<sup>32</sup> and they exhibited a sphere morphology (Figure 2A). Then, the direct growth of ZIF-8 was observed with the transmission electron microscopy (TEM) images, and the size of PB nanoparticles increased with formation of the ZIF-8 agglomeration layer. Elemental mapping images of the MPBZC specimens revealed the presence of Fe and Zn in the MPBZC nanoparticles (Figure 2B). From the X-ray diffraction (XRD) patterns in Figure 2C and the X-ray photoelectron spectroscopy (XPS) results in





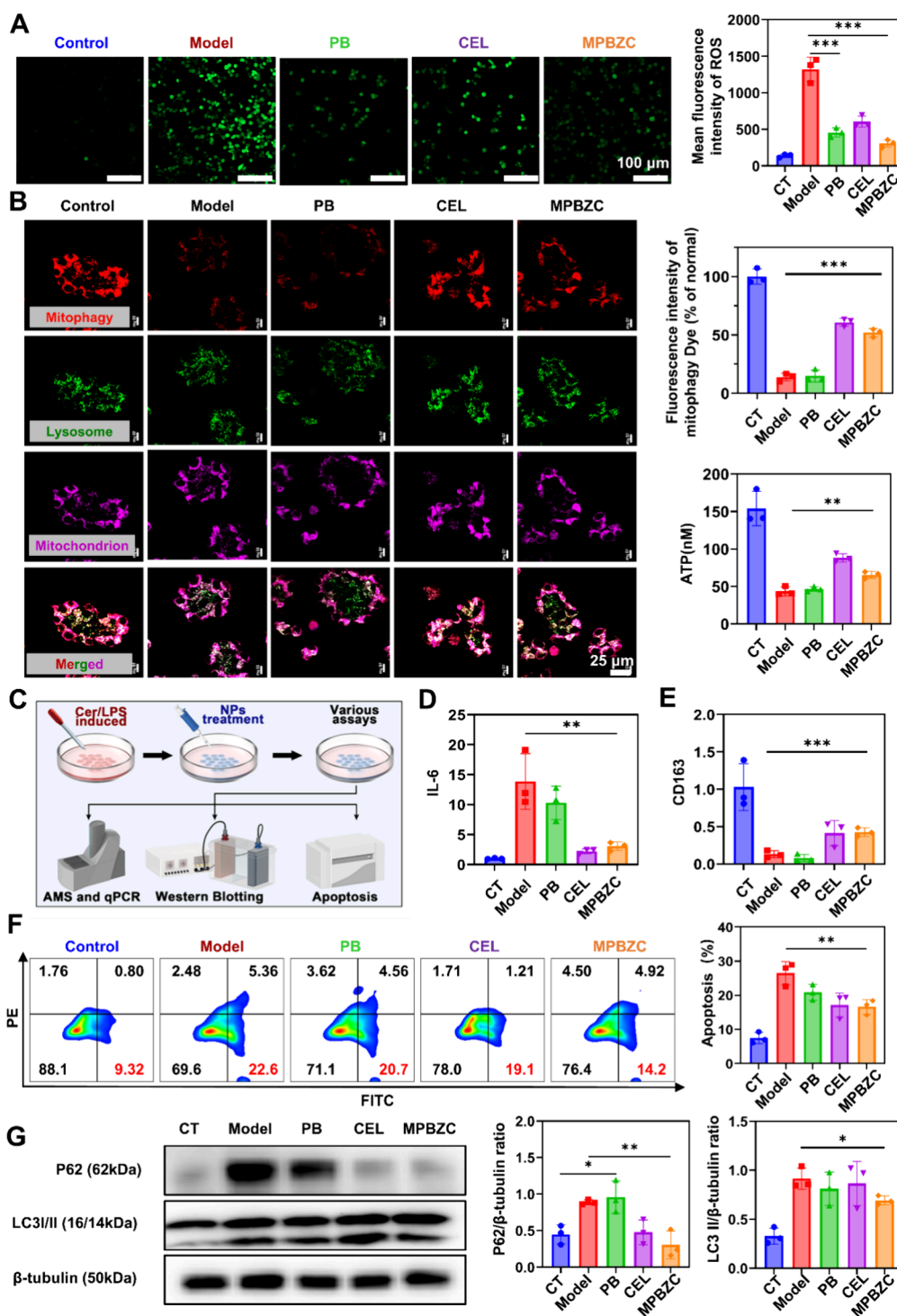
**Figure 3.** pH-responsive ability and free-radical scavenging capacity of MPBZC. (A) TEM images of MPBZC incubated in solutions with a pH of 5.5 at different times (scale bar = 100 nm). (B) Size distribution of MPBZC incubated with solutions of different pH. (C) SOD-like activities of PB, CEL, PBZ, PBZC, and MPBZC. (D) CAT-like activities of PB, CEL, PBZ, PBZC, and MPBZC. (E) Images of the H<sub>2</sub>O<sub>2</sub> reaction after the addition of PB, CEL, PBZ, PBZC, and MPBZC. (F) POD-like activity of PB, CEL, PBZ, PBZC, and MPBZC. (G) DPPH as a substrate to detect nitrogen radical inhibition by PB, CEL, PBZ, PBZC, and MPBZC. (H) Schematic representation of the ROS/RNS scavenging capacity of MPBZC.

Figure 2D, PBZC presented several characteristic peaks that corresponded to PB nanoparticles and ZIF-8, confirming the successful formation of a hierarchical ZIF-8 layer on the surface of PB nanoparticles. As the heterostructure shell, ZIF-8 has abundant large pores, and the hydrophobic drug was loaded effectively through  $\pi$ - $\pi$ -stacking and hydrogen-bonding interactions. As present in Figure 2E, the celastrol-loaded PBZC had typical celastrol characteristic absorbance peaks at 425 and 695 nm, indicating that celastrol was loaded into the PBZC successfully. To improve the targeting ability of PBZC, the macrophage cell membrane was harvested. As shown in the TEM image, the shell structure on the surface of nanoparticles and the increased size indicated that the coating of the cell membrane on PBZC was successful. Moreover, the sodium dodecyl sulfate–polyacrylamide gel electrophoresis assay showed that both the macrophage cell membrane and MPBZC contained proteins from RAW264.7, indicating that membrane proteins still existed in the MPBZC after extrusion (Figure 2F). CD44, the key marker of the macrophage cell surface involved in targeting, was verified by Western blot analysis (Figure 2G). As shown in Figure 2H, dynamic light scattering (DLS) analysis indicated that the hydrodynamic diameter of MPBZC was 220 nm. Compared with uncoated PBZC, the  $\zeta$  potential of MPBZC decreased from  $-8.99$  to  $-16.73$  mV, indicating the successful encapsulation of MPBZC (Figure 2I). Furthermore, the stability of MPBZC was evaluated in various physiological media (Figure S1), and the DLS results and corresponding scanning electron microscopy (SEM) images indicated that MPBZC maintained their structure over 7 days, validating the stability of MPBZC.

Constructing an inflammatory microenvironment responsive nanosystem to deliver drugs can effectively improve the therapeutic effect of severe inflammatory diseases.<sup>33–35</sup> The inflammatory microenvironment is characterized by weakly acidic conditions. ZIF-8 possesses acidity-triggered degradability, a key feature for its potential applications in drug-delivery systems.<sup>36,37</sup> The MPBZC consisted of a ZIF-8-coated PB core, which could serve as a highly effective “turn-on” tool for precisely treating SAP. The TEM images indicated that the structure of MPBZC was degraded over time in acidic conditions (Figure 3A). DLS further confirmed that the distribution of MPBZC, in terms of the hydrodynamic size, was divided into two peaks in a weakly acidic solution (pH 5.5) over time (Figure 3B).

As the outer ZIF-8 shell degraded and the drug was released, the inner PB core was exposed, which acts as an artificial nanoenzyme to catalyze the detrimental ROS enriched in the inflammatory microenvironment into harmless H<sub>2</sub>O and O<sub>2</sub>.<sup>38–41</sup> As exhibited in Figure 3C, the superoxide dismutase (SOD)-like activity of PB, PBZ, PBZC, and MPBZC was measured, and all showed excellent SOD-like catalytic activity. Because the half-life of O<sub>2</sub><sup>•-</sup> and •OH are short, the concentration of H<sub>2</sub>O<sub>2</sub> is highest among the biologically relevant ROS.<sup>42</sup> Because catalase (CAT) is responsible for the catalytic reaction of H<sub>2</sub>O<sub>2</sub> to generate O<sub>2</sub>,<sup>43</sup> the CAT mimetic activity was measured. Figure 3D showed that the concentration of O<sub>2</sub> increased significantly with the addition of MPBZC, which is due to the CAT mimetic activity of PB. Furthermore, plenty of O<sub>2</sub> bubbles were observed by adding H<sub>2</sub>O<sub>2</sub> to the MPBZC solution (Figure 3E). A classical chromogenic reaction has been implemented to detect





**Figure 4.** MPBZC alleviate inflammation and cell apoptosis by restoring impaired mitochondrial autophagic flux and scavenging ROS in vitro. (A) Evaluation of ROS generation and fluorescence semiquantification under treatments of PB (25  $\mu\text{g}/\text{mL}$ ), CEL (10  $\mu\text{g}/\text{mL}$ ), and MPBZC (e.g., [PB] = 25  $\mu\text{g}/\text{mL}$  and [CEL] = 10  $\mu\text{g}/\text{mL}$ ) by dichlorofluorescein (DCF) measurement using confocal microscopy (scale bar = 100  $\mu\text{m}$ ). (B) Evaluation of mitochondrial autophagy under treatments of PB (25  $\mu\text{g}/\text{mL}$ ), CEL (10  $\mu\text{g}/\text{mL}$ ), and MPBZC (e.g., [PB] = 25  $\mu\text{g}/\text{mL}$  and [CEL] = 10  $\mu\text{g}/\text{mL}$ ) using confocal microscopy. Mitochondrial autophagy is indicated by the red probe, and lysosomes are indicated by the green probe (scale bar = 25  $\mu\text{m}$ ). Fluorescence semiquantification of the mitochondrial autophagy levels under different treatments using confocal microscopy. ATP production under different treatments. (C) Schematic diagram of the in vitro experiments. (D) mRNA expression levels of IL-6 (D) and CD163 (E) under different treatments ( $n = 3$ ). (F) Apoptosis of cerulein + LPS-induced AR42J cells after different treatments. The cells were stained using an Annexin V-FITC/PI kit and analyzed by flow cytometry ( $n = 3$ ). (G) Quantitative analysis and Western blot images of P62 and LC3 II/I in AR42J cells under different treatments. The results are presented as mean  $\pm$  SD,  $n = 3$ . \* $p < 0.05$ , \*\* $p < 0.01$ , and \*\*\* $p < 0.001$ .

MPBZC's peroxidase (POD)-like activity. With the addition of MPBZC, colorless 2,2'-azinobis(3-ethylbenzothiazoline-6-sul-

fonic acid) oxidized quickly and absorbance increased significantly (Figure 3F). Moreover, \*DPPH is a highly stable

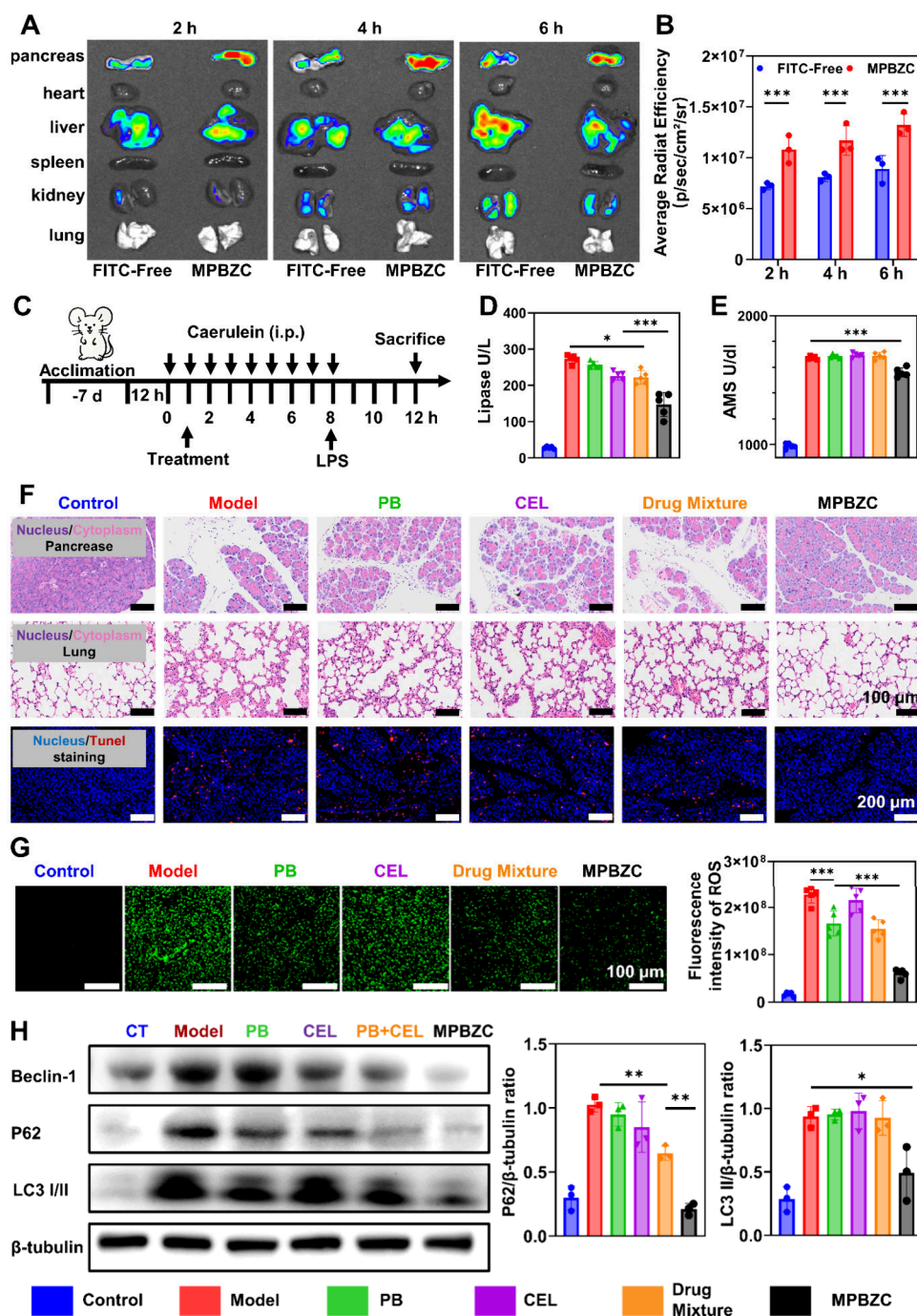


**Figure 5.** Treatment of MPBZC alleviating inflammation in the cerulein + LPS-induced SAP animal model by restoring impaired mitochondrial autophagic flux and scavenging of ROS. (A) Representative ex vivo images of major organs at different time points after tail vein injection of various reagents in SAP mice,  $n = 3$ . (B) Semiquantitative analysis of total fluorescence signals detected ex vivo in major organs after tail vein injection of various reagents in SAP mice (ARE = average radiation efficiency). Data are mean  $\pm$  SD,  $n = 3$ . (C) Experimental flowchart of the treatment process. Serum levels of lipase (D) and amylase (E) after tail vein injection of various reagents in SAP mice, including Control (CT), cerulein + LPS (model), cerulein + LPS + PB (PB, 2.5 mg/kg), cerulein + LPS + CEL (CEL, 1 mg/kg), cerulein + LPS + drug mixture of PB and CEL (drug mixture of, e.g., [PB] = 2.5 mg/kg and [CEL] = 1 mg/kg), and cerulein + LPS + MPBZC (MPBZC, e.g., [PB] = 2.5 mg/kg and [CEL] = 1 mg/kg),  $n = 5$ . (F) Representative images of H&E-stained pancreatic and lung tissue samples after tail vein injection of various reagents in SAP mice (scale bar = 100  $\mu$ m) and confocal microscopy images of TUNEL-stained pancreatic tissue after tail vein injection of various reagents in SAP mice. Scale bar: 200  $\mu$ m. (G) Evaluation of ROS generation and fluorescence semiquantification in pancreatic samples of SAP mice under different treatments by DCF measurement using confocal microscopy ( $n = 3$ ). (H) Quantitative analysis and Western blot images of Beclin-1, P62, and LC3 I/II in pancreatic tissues from cerulein + LPS-induced SAP models under different treatments, with  $\beta$ -tubulin as the loading control ( $n = 3$ ). The results are presented as mean  $\pm$  SD. \* $p < 0.05$ , \*\* $p < 0.01$ , and \*\*\* $p < 0.001$ .

and most commonly used free radical for evaluating the ability to capture reactive nitrogen species.<sup>44</sup> After incubation with MPBZC, •DPPH radicals were inhibited remarkably (Figure

3G). The results indicated that MPBZC is a promising candidate for scavenging ROS in the treatment of SAP (Figure 3H).

The toxicity and uptake efficiency of PB and MPBZC in the acinar cells were measured. As shown in Figure S2A,B, minimal cytotoxicity was observed in AR42J cells. Then, the AR42J cell uptake efficiency of MPBZC was measured by using flow cytometry and laser confocal microscopy. The value increased to 63.7% at 1 h and exceeded 90% at 4 h (Figure S2C). Moreover, the overlap between the lysosome and fluorescein isothiocyanate (FITC)-labeled MPBZC increased, indicating that nearly all acinar cells had completed the uptake of MPBZC via the endolysosomal pathway within 4 h (Figure S2D,E). Significant ROS accumulation was detected in the SAP cell model by the ROS probe. The fluorescence intensity of ROS decreased by 43% after the addition of MPBZC (Figure S3A). Results from confocal laser scanning microscopy confirmed the scavenging of ROS in the MPBZC group (Figure 4A). Furthermore, after treatment with MPBZC, the concentration of glutathione, SOD, and malondialdehyde increased significantly (Figure S3B,D).

Depolarization of the mitochondrial membrane potential ( $\Delta\psi_m$ ) leads to impaired adenosine triphosphate (ATP) synthesis and cellular energy depletion, while decreased mitochondrial autophagy exacerbates the accumulation of mitochondrial damage.<sup>4</sup> Acinar cells were exposed to cerulein and lipopolysaccharide (LPS) to simulate the inflammatory microenvironment of SAP. A significant reduction in the fluorescence intensity of tetramethylrhodamine ethyl ester (TMRE) was observed as the fluorescence decreased by approximately 74%. However, the treatment of PB alone could not reverse the depolarization of  $\Delta\psi_m$ , indicating substantial mitochondrial membrane potential damage accumulating in acinar cells around the inflammatory environment of SAP, which could not be restored by simply eliminating ROS. By loading of CEL, MPBZC showed a great ability to regulate  $\Delta\psi_m$ . Similar trends were observed by using the JC-1 mitochondrial membrane potential probe (Figure S5).

The depolarization of  $\Delta\psi_m$  is the most critical initiation event among the several triggers of mitophagy.<sup>21</sup> Subsequently, we explored whether depolarization of  $\Delta\psi_m$  facilitates mitophagy in the inflammatory microenvironment of SAP. Laser confocal microscopy scanning revealed a significant decrease in the mitochondrial autophagy levels in the model group, with the fluorescence intensity decreasing to 13.91% compared with the control group. The addition of PB has no influence on the mitophagy of AR42J cells, with a fluorescence intensity of mitophagy dye of only 14.93%. However, the fluorescence intensity of the mitophagy dye increased by 4.3- and 3.7-fold with the treatment of CEL and MPBZC (Figure 4B). The ATP production under SAP conditions was measured further. The results showed that, after the treatment of MPBZC, the production efficiency of ATP in acinar cells increased from 28% to 42% compared with the control group. Ineffective clearance of damaged mitochondria caused by impaired autophagy in the SAP inflammatory microenvironment leads to pancreatic tissue necrosis and localized inflammation.<sup>45</sup> As a ligand of nuclear receptor Nur77, celastrol promotes Nur77 migration from the nucleus to mitochondria, improving mitophagy and promoting the cellular repair of damaged mitochondria.<sup>46</sup> By loading celastrol, MPBZC recovered the normal mitochondrial membrane potential and restored mitochondrial autophagy function, serving as an effective therapeutic strategy to alleviate SAP.

AR42J cells were exposed to cerulein and LPS to simulate the SAP environment (Figure 4C). The results showed that

the amylase level in acinar cells increased 1.69-fold and the apoptosis rate increased from 9.3% to 22.6% compared with the control group. With the treatment of MPBZC, the amylase level in the culture medium decreased by 70% (Figure S6). Furthermore, the mRNA expression of inflammatory cytokines TNF- $\alpha$ , IL-6, IL-1 $\beta$ , and iNOS and anti-inflammatory factor CD163 was measured (Figures 4D,E and S6). Treatment with MPBZC exhibited excellent anti-inflammatory effects. The cell apoptosis was detected by Annexin V/PE assay. The result showed that the apoptosis rate in the model group increased to 22.6%. With the addition of MPBZC, the apoptosis rate decreased to 14.2% (Figure 4F). Impaired autophagic flux leads to the accumulation of damaged mitochondria, which is one of SAP's most crucial pathological progression.<sup>47</sup> LC3, P62, Pink1, and Parkin8 are key molecules in the mitophagy.<sup>48</sup> The expression of Pink1 and Parkin8 in AR42J cells was reduced by 28% and 46%, respectively, in the SAP cell model. The addition of PB showed little influence on the expression of Pink1 and Parkin8, indicating that mitophagy dysfunction in SAP cannot be reversed by simply alleviating ROS (Figure S7). The protein expression levels of P62 and LC3 II/I increased by 2.8-fold and 1.9-fold in the model group, confirming that while the initiation stage of autophagy is activated in acinar cells under the SAP inflammatory microenvironment, the completion stage is inhibited, leading to the impaired autophagic flux. The addition of MPBZC reduced the expression of P62 and LC3 II/I significantly, indicating that MPBZC restored mitophagy inhibition and autophagic flux damage (Figure 4G).

With the coating of the macrophage membrane, the celastrol delivery system has the potential ability to target the inflammation of SAP tissues. The distribution of MPBZC in vivo was evaluated by intravenous injection of FITC-labeled MPBZC in the SAP mouse model. The fluorescence intensity of MPBZC in the pancreas was significantly higher (1.5-fold) 2 h after the injection. Interestingly, in the mice without the treatment of cerulein and LPS, there was no difference in the accumulation of MPBZC and free FITC in various organs (Figures S4A,B and S8), indicating that MPBZC accumulates and is retained in pancreatic tissue by targeting the inflamed areas of the pancreas under the inflammatory condition of SAP. Celastrol is acknowledged as one of the natural extracts with the highest therapeutic potential for clinical treatment.<sup>49</sup> However, severe systemic toxicity impedes its clinical utility.<sup>50,51</sup> A variety of MPBZC solutions loaded with different concentrations of celastrol were injected into the mice. Blood routine and blood biochemistry examination indicated that the optimal dose of celastrol was 1 mg/kg (Figure S9).

As shown in Figure 5C, serum analysis revealed that the amylase and lipase levels in the model group were remarkably increased. The levels of the inflammatory cytokines TNF- $\alpha$ , IL-6, and IL-1 $\beta$  were also significantly upregulated. Histological examination of the pancreas and lungs showed a pronounced infiltration of inflammatory cells and pancreatic cell necrosis. The levels of amylase and lipase decreased by 52% and 47% after the treatment of MPBZC (Figure S4D,E). Additionally, the levels of the inflammatory cytokines TNF- $\alpha$ , IL-6, and IL-1 $\beta$  were reduced (Figure S10). Histological examination of pancreatic and lung tissues from MPBZC-treated mice showed that pancreatic edema was reduced, infiltration of inflammatory cells gradually decreased, and the area of the inflammatory region was smaller in the MPBZC-treated group. Additionally, the alveolar walls showed a more regular structure, and the cells were restored to their normal morphology. After



treatment with MPBZC, the proportion of apoptotic cells decreased by 81% (Figures S5F and S11). To more rigorously assess proliferation, the tissues were stained with Ki-67. The relative fluorescence intensity of Ki-67 increased significantly (4.2-fold), indicating that the damaged acinar cells were replaced by newly proliferated acinar cells due to the treatment of MPBZC (Figure S12). Furthermore, MPBZC was labeled with FITC, and colocalization analysis was conducted; the overlap of fluorescence demonstrated that the therapeutic effect was achieved with the treatment of MPBZC. The alcoholic SAP model and the CDE-induced (choline-deficient and supplemented with ethionine diet) SAP model were further employed to investigate the therapeutic effects of MPBZC on different types of SAP. As shown in Figures S13 and S14, the treatment of MPBZC enhanced the therapeutic effect, with the amylase and lipase decreased and decreased pancreatic damage sites and apoptosis rate. In addition, the mice exhibited a near 100% mortality rate within 7 days in the CDE-induced SAP model group. The treatment of MPBZC significantly improved the 7-day survival rate from approximately 10% to 60%. Notably, CDE mice treated with MPBZC maintained a 50% survival rate for 20 days.

Subsequently, ROS was detected in the pancreatic tissue of mice, and the results showed that the fluorescence intensity in the pancreatic tissue of the model group was 13.7 times higher than that in the control group. The treatment of MPBZC significantly eliminated the ROS by 74% (Figure S5G). Furthermore, CEL loading in MPBZC was introduced to restore the impaired autophagic flux. As shown in Figure S5H, the expression of autophagy-related proteins in the pancreatic tissue was significantly increased in the SAP mouse model, with the protein expression levels of Beclin-1, LC3II/I, and P62 were 1.86, 3.27, and 3.43 times higher than those in the control group. The treatment of MPBZC reduced the protein expression of Beclin-1, LC3II/I, and P62, which decreased significantly to 39%, 52%, and 20%. In the alcoholic pancreatitis model, these levels decreased by 30%, 64%, and 53% (Figure S15). To further verify this mechanism, mitochondria were isolated from the pancreas of mice to detect the expression of autophagic-flux-related proteins. The results exhibited that the addition of MPBZC activated the translocation of Nur77 to the mitochondria and promoted mitophagy (Figure S16). These results further confirmed that an excellent therapeutic effect on SAP was obtained by the combination treatment of scavenging excessive ROS and restoring impaired autophagic flux.

Assessing the biosafety of MPBZC is a critical step before clinical application. Hematological analysis demonstrated no notable alterations among healthy mice treated with MPBZC, CEL, or PB, compared with the control group. Similarly, biochemical indices remained within normal ranges across all experimental groups (Figure S17). Histological examination of major organs revealed no observable pathological abnormalities in the treated mice (Figure S18). To further validate the biological safety of the MPBZC, organ histopathology, immune responses, and long-term biodistribution were assessed (Figures S19 and S20). The results demonstrated that the MPBZC formulation is nontoxic and has favorable biosafety for potential applications.

In this study, we have successfully developed a novel biomimetic nanozyme MPBZC for the treatment of SAP. This innovative nanosystem integrates the ROS scavenging capabilities of PB with the autophagy-promoting effects of

CEL, encapsulated within a porous ZIF-8 shell and coated with a macrophage membrane for targeted delivery to inflamed pancreatic tissues. The design of MPBZC represents a significant advancement in multitargeted synergistic treatment strategies, addressing both the excessive production of ROS and impaired mitochondrial function, which are critical pathological features of SAP.

## ■ ASSOCIATED CONTENT

### SI Supporting Information

The Supporting Information is available free of charge at <https://pubs.acs.org/doi/10.1021/acs.nanolett.5c01495>.

Experimental materials and characterization methods, enzyme-like activity test, cell culture and treatment, cytotoxicity assay, subcellular distribution, detection of the mitochondrial membrane potential, mitophagy, and ATP production, cell apoptosis detection; animal experimentation; histopathology and pathological scoring; determination of serum amylase, lipase, and inflammatory factors; biodistribution of MPBZC; terminal deoxynucleotidyl transferase dUTP nick-end labeling (TUNEL) assay; protein extraction and Western blotting; RNA extraction and real-time quantitative PCR; analysis of oxidative-stress-related factors; evaluation of biosafety; in vitro uptake efficiency of MPBZC; antioxidant capacity of MPBZC; MPBZC restores damaged mitochondrial membrane potential; evaluation of the mitochondrial membrane potential using the JC-1 fluorescent probe; MPBZC alleviates SAP inflammation in vitro; MPBZC alleviates inflammation by restoring impaired mitochondrial autophagic flux in vitro; study of MPBZC accumulation and targeting in the pancreas of normal mice in vivo; MPBZC treatment in the cerulein + LPS-induced SAP animal model; MPBZC treatment on the mouse models of alcoholic pancreatitis; MPBZC treatment on the mouse models of CDE diet pancreatitis; MPBZC restores impaired autophagic flux through the LC3 II/I-P62-mediated signaling pathway; representative H&E-stained images of major organs; and biosafety evaluation (PDF)


## ■ AUTHOR INFORMATION

### Corresponding Authors

**Xin Yu** – Department of General Surgery, Sir Run Run Shaw Hospital, School of Medicine, Zhejiang University, Hangzhou, Zhejiang 310016, People's Republic of China; Zhejiang Key Laboratory of Precise Diagnosis and Treatment of Abdominal Infection, Sir Run Run Shaw Hospital, School of Medicine and Department of Anesthesia, Sir Run Run Shaw Hospital, Zhejiang University, Hangzhou, Zhejiang 310016, People's Republic of China; [orcid.org/0000-0002-6967-8704](https://orcid.org/0000-0002-6967-8704); Email: [xinxin\\_yu@zju.edu.cn](mailto:xinxin_yu@zju.edu.cn)

**Hong Yu** – Department of General Surgery, Sir Run Run Shaw Hospital, School of Medicine, Zhejiang University, Hangzhou, Zhejiang 310016, People's Republic of China; Zhejiang Key Laboratory of Precise Diagnosis and Treatment of Abdominal Infection, Sir Run Run Shaw Hospital, School of Medicine, Zhejiang University, Hangzhou, Zhejiang 310016, People's Republic of China; Email: [blueyu000@zju.edu.cn](mailto:blueyu000@zju.edu.cn)

**Dong Cen** – Department of General Surgery, Sir Run Run Shaw Hospital, School of Medicine, Zhejiang University,

Hangzhou, Zhejiang 310016, People's Republic of China;  
 [orcid.org/0009-0006-9161-253X](https://orcid.org/0009-0006-9161-253X); Email: [dongcen@zju.edu.cn](mailto:dongcen@zju.edu.cn)

## Authors

**Liyang Wang** – Department of General Surgery, Sir Run Run Shaw Hospital, School of Medicine, Zhejiang University, Hangzhou, Zhejiang 310016, People's Republic of China; Zhejiang Key Laboratory of Precise Diagnosis and Treatment of Abdominal Infection, Sir Run Run Shaw Hospital, School of Medicine, Zhejiang University, Hangzhou, Zhejiang 310016, People's Republic of China

**Zerui Gao** – Department of General Surgery, Sir Run Run Shaw Hospital, School of Medicine, Zhejiang University, Hangzhou, Zhejiang 310016, People's Republic of China; Zhejiang Key Laboratory of Precise Diagnosis and Treatment of Abdominal Infection, Sir Run Run Shaw Hospital, School of Medicine, Zhejiang University, Hangzhou, Zhejiang 310016, People's Republic of China

**Mengxiang Tian** – Department of General Surgery, Sir Run Run Shaw Hospital, School of Medicine, Zhejiang University, Hangzhou, Zhejiang 310016, People's Republic of China; Zhejiang Key Laboratory of Precise Diagnosis and Treatment of Abdominal Infection, Sir Run Run Shaw Hospital, School of Medicine, Zhejiang University, Hangzhou, Zhejiang 310016, People's Republic of China

**Li Liu** – Department of General Surgery, Sir Run Run Shaw Hospital, School of Medicine, Zhejiang University, Hangzhou, Zhejiang 310016, People's Republic of China; Zhejiang Key Laboratory of Precise Diagnosis and Treatment of Abdominal Infection, Sir Run Run Shaw Hospital, School of Medicine, Zhejiang University, Hangzhou, Zhejiang 310016, People's Republic of China

**Jinyan Xie** – Department of General Surgery, Sir Run Run Shaw Hospital, School of Medicine, Zhejiang University, Hangzhou, Zhejiang 310016, People's Republic of China; Zhejiang Key Laboratory of Precise Diagnosis and Treatment of Abdominal Infection, Sir Run Run Shaw Hospital, School of Medicine, Zhejiang University, Hangzhou, Zhejiang 310016, People's Republic of China

**Muxiong Chen** – Department of General Surgery, Sir Run Run Shaw Hospital, School of Medicine, Zhejiang University, Hangzhou, Zhejiang 310016, People's Republic of China; Zhejiang Key Laboratory of Precise Diagnosis and Treatment of Abdominal Infection, Sir Run Run Shaw Hospital, School of Medicine, Zhejiang University, Hangzhou, Zhejiang 310016, People's Republic of China

**Zihao Huang** – Department of General Surgery, Sir Run Run Shaw Hospital, School of Medicine, Zhejiang University, Hangzhou, Zhejiang 310016, People's Republic of China; Zhejiang Key Laboratory of Precise Diagnosis and Treatment of Abdominal Infection, Sir Run Run Shaw Hospital, School of Medicine, Zhejiang University, Hangzhou, Zhejiang 310016, People's Republic of China

**Bingzhi Dong** – Department of General Surgery, Sir Run Run Shaw Hospital, School of Medicine, Zhejiang University, Hangzhou, Zhejiang 310016, People's Republic of China; Zhejiang Key Laboratory of Precise Diagnosis and Treatment of Abdominal Infection, Sir Run Run Shaw Hospital, School of Medicine, Zhejiang University, Hangzhou, Zhejiang 310016, People's Republic of China

**Weiqli Li** – Department of General Surgery, Sir Run Run Shaw Hospital, School of Medicine, Zhejiang University, Hangzhou,

Zhejiang 310016, People's Republic of China; Zhejiang Key Laboratory of Precise Diagnosis and Treatment of Abdominal Infection, Sir Run Run Shaw Hospital, School of Medicine, Zhejiang University, Hangzhou, Zhejiang 310016, People's Republic of China

**Liang Shi** – Department of General Surgery, Sir Run Run Shaw Hospital, School of Medicine, Zhejiang University, Hangzhou, Zhejiang 310016, People's Republic of China

**Yifan Tong** – Department of General Surgery, Sir Run Run Shaw Hospital, School of Medicine, Zhejiang University, Hangzhou, Zhejiang 310016, People's Republic of China; Zhejiang Key Laboratory of Precise Diagnosis and Treatment of Abdominal Infection, Sir Run Run Shaw Hospital, School of Medicine, Zhejiang University, Hangzhou, Zhejiang 310016, People's Republic of China

**Hongxia Xu** – Department of General Surgery, Sir Run Run Shaw Hospital, School of Medicine, Zhejiang University, Hangzhou, Zhejiang 310016, People's Republic of China

**Bo Shen** – Department of General Surgery, Sir Run Run Shaw Hospital, School of Medicine, Zhejiang University, Hangzhou, Zhejiang 310016, People's Republic of China; Zhejiang Key Laboratory of Precise Diagnosis and Treatment of Abdominal Infection, Sir Run Run Shaw Hospital, School of Medicine, Zhejiang University, Hangzhou, Zhejiang 310016, People's Republic of China

Complete contact information is available at:

<https://pubs.acs.org/10.1021/acs.nanolett.5c01495>

## Author Contributions

<sup>†</sup>L.W., Z.G., and M.T. contributed equally to this work.

## Notes

The authors declare no competing financial interest.

## ACKNOWLEDGMENTS

This research was supported by the Zhejiang Provincial Natural Science Foundation of China (No. LQ24E030004), the Zhejiang Province Medical and Health Technology Project (No. 2024653117), the Key Scientific Research Program of Hangzhou (No. 2024SZD1B06), the Science and Technology Program of Zhejiang Province (No. 2024C03201, 2025C02133), the Co-construction Science and Technology Program of Zhejiang Traditional Chinese Medicine Administration (GZY-ZJ-KJ-24032), the National Natural Science Foundation of China (Nos. 82270670 and 82470669), the Central Government Guides Local Science and Technology Development Fund Projects (No. 2024ZY01020), the Zhejiang Medical Health Science and Technology Program (No. 2023RC031), and the Zhejiang Provincial Natural Science Foundation of China (No. LMS25H160008).

## REFERENCES

- (1) Ammer-Herrmenau, C.; Antweiler, K. L.; Asendorf, T.; Beyer, G.; Buchholz, S. M.; Cameron, S.; Capurso, G.; Damm, M.; Dang, L.; Frost, F.; Gomes, A.; Hamm, J.; Henker, R.; Hoffmeister, A.; Meinhardt, C.; Nawacki, L.; Nunes, V.; Panyko, A.; Pardo, C.; Phillip, V.; Pukitis, A.; Rasch, S.; Riekstina, D.; Rinja, E.; Ruiz-Rebollo, M. L.; Sirtl, S.; Weingarten, M.; Sandru, V.; Woitalla, J.; Ellenrieder, V.; Neeße, A. Gut microbiota predicts severity and reveals novel metabolic signatures in acute pancreatitis. *Gut* **2024**, 73 (3), 485–495.
- (2) Aney, K. J.; Jeong, W. J.; Vallejo, A. F.; Burdziak, C.; Chen, E.; Wang, A.; Koak, P.; Wise, K.; Jensen, K.; Pe'er, D.; Dougan, S. K.; Martelotto, L.; Nissim, S. Novel Approach for Pancreas Tran-



scriptomics Reveals the Cellular Landscape in Homeostasis and Acute Pancreatitis. *Gastroenterology* **2024**, *166* (6), 1100–1113.

(3) Alexander, V. J.; Karwatowska-Prokopczuk, E.; Prohaska, T. A.; Li, L.; Geary, R. S.; Gouni-Berthold, I.; Oral, E. A.; Hegele, R. A.; Stroes, E. S. G.; Witztum, J. L.; Tsimikas, S. Volanesorsen to Prevent Acute Pancreatitis in Hypertriglyceridemia. *N. Engl. J. Med.* **2024**, *390* (5), 476–477.

(4) Biczó, G.; Vegh, E. T.; Shalbueva, N.; Mareninova, O. A.; Elperin, J.; Lotshaw, E.; Gretler, S.; Lugea, A.; Malla, S. R.; Dawson, D.; Ruchala, P.; Whitelegge, J.; French, S. W.; Wen, L.; Husain, S. Z.; Gorelick, F. S.; Hegyi, P.; Rakonczay, Z., Jr.; Gukovsky, I.; Gukovskaya, A. S. Mitochondrial Dysfunction, Through Impaired Autophagy, Leads to Endoplasmic Reticulum Stress, Deregulated Lipid Metabolism, and Pancreatitis in Animal Models. *Gastroenterology* **2018**, *154* (3), 689–703.

(5) Zi, Z.; Rao, Y. Discoveries of GPR39 as an evolutionarily conserved receptor for bile acids and of its involvement in biliary acute pancreatitis. *Sci. Adv.* **2024**, *10* (5), No. ead0146, DOI: 10.1126/sciadv.ad0146.

(6) Marchi, S.; Guilbaud, E.; Tait, S. W. G.; Yamazaki, T.; Galluzzi, L. Mitochondrial control of inflammation. *Nature Reviews Immunology* **2023**, *23* (3), 159–173.

(7) Habtezion, A.; Gukovskaya, A. S.; Pandol, S. J. Acute Pancreatitis: A Multifaceted Set of Organelle and Cellular Interactions. *Gastroenterology* **2019**, *156* (7), 1941–1950.

(8) Garg, P. K.; Singh, V. P. Organ Failure Due to Systemic Injury in Acute Pancreatitis. *Gastroenterology* **2019**, *156* (7), 2008–2023.

(9) Xie, X.; Zhao, J. L.; Gao, W.; Chen, J.; Hu, B.; Cai, X. J.; Zheng, Y. Y. Prussian blue nanozyme-mediated nanoscavenger ameliorates acute pancreatitis via inhibiting TLRs/NF- $\kappa$ B signaling pathway. *Theranostics* **2021**, *11* (7), 3213–3228.

(10) Vollmar, B.; Menger, M. D. Microcirculatory dysfunction in acute pancreatitis. A new concept of pathogenesis involving vasomotion-associated arteriolar constriction and dilation. *Pancreatology* **2003**, *3* (3), 181–190.

(11) Zhang, X. P.; Li, Z. J.; Zhang, J. Inflammatory mediators and microcirculatory disturbance in acute pancreatitis. *Hepatobiliary Pancreat. Dis. Int.* **2009**, *8* (4), 351–357.

(12) Zhang, B. S.; Wang, C.; Guo, M. Y.; Zhu, F. X.; Yu, Z. Q.; Zhang, W. X.; Li, W. Y.; Zhang, Y. J.; Tian, W. M. Circadian Rhythm-Dependent Therapy by Composite Targeted Polyphenol Nanoparticles for Myocardial Ischemia-Reperfusion Injury. *ACS Nano* **2024**, *18* (41), 28154–28169.

(13) Wang, D. X.; Wang, T. T.; Zhang, Z. H.; Li, Z. M.; Guo, Y. X.; Zhao, G. S.; Wu, L. Recent advances in the effects of dietary polyphenols on inflammation potential molecular mechanisms, receptor targets, safety issues, and uses of nanodelivery system and polyphenol polymers. *Curr. Opin. Food Sci.* **2022**, *48*, 100921.

(14) Tao, W. Y.; Zhang, Y.; Shen, X. M.; Cao, Y. P.; Shi, J.; Ye, X. Q.; Chen, S. G. Rethinking the Mechanism of the Health Benefits of Proanthocyanidins: Absorption, Metabolism, and Interaction with Gut Microbiota. *Compr. Rev. Food Sci. F* **2019**, *18* (4), 971–985.

(15) Shi, H. X.; Guo, Y. Y.; Geng, C.; Chen, L.; He, S.; He, W. X.; Chen, Y. B.; Chan, Y. K.; Wang, C. H.; Deng, Y. Engineered Bio-Heterojunction with Robust ROS-Scavenging and Anti-Inflammation for Targeted Acute Pancreatitis Therapy. *Adv. Funct. Mater.* **2024**, *35* (3), 2413276.

(16) Wang, Y. A.; Wang, X. Y.; Zhang, X.; Zhang, B. M.; Meng, X. L.; Qian, D. Y.; Xu, Y. T.; Yu, L. M.; Yan, X. F.; He, Z. Y. Inflammation and Acinar Cell Dual-Targeting Nanomedicines for Synergistic Treatment of Acute Pancreatitis via Ca<sup>2+</sup> Homeostasis Regulation and Pancreas Autodigestion Inhibition. *ACS Nano* **2024**, *18* (18), 11778–11803.

(17) Levine, B.; Kroemer, G. Biological Functions of Autophagy Genes: A Disease Perspective. *Cell* **2019**, *176* (1–2), 11–42.

(18) Klionsky, D. J.; Petroni, G.; Amaravadi, R. K.; Baehrecke, E. H.; Ballabio, A.; Boya, P.; Bravo-San Pedro, J. M.; Cadwell, K.; Cecconi, F.; Choi, A. M. K.; Choi, M. E.; Chu, C. T.; Codogno, P.; Colombo, M. I.; Cuervo, A. M.; Deretic, V.; Dikic, I.; Elazar, Z.; Eskelinen, E. L.;

Fimia, G. M.; Gewirtz, D. A.; Green, D. R.; Hansen, M.; Jäättelä, M.; Johansen, T.; Juhász, G.; Karantza, V.; Kraft, C.; Kroemer, G.; Ktistakis, N. T.; Kumar, S.; Lopez-Otin, C.; Macleod, K. F.; Madeo, F.; Martinez, J.; Meléndez, A.; Mizushima, N.; Münz, C.; Penninger, J. M.; Perera, R. M.; Piacentini, M.; Reggiori, F.; Rubinsztein, D. C.; Ryan, K. M.; Sadoshima, J.; Santambrogio, L.; Scorrano, L.; Simon, H. U.; Simon, A. K.; Simonsen, A.; Stolz, A.; Tavernarakis, N.; Tooze, S. A.; Yoshimori, T.; Yuan, J.; Yue, Z.; Zhong, Q.; Galluzzi, L.; Pietrocola, F. Autophagy in major human diseases. *EMBO J.* **2021**, *40* (19), No. e108863.

(19) Yang, L.; Ye, F.; Liu, J.; Klionsky, D. J.; Tang, D.; Kang, R. Extracellular SQSTM1 exacerbates acute pancreatitis by activating autophagy-dependent ferroptosis. *Autophagy* **2023**, *19* (6), 1733–1744.

(20) Zhang, Z.; Yue, P.; Lu, T.; Wang, Y.; Wei, Y.; Wei, X. Role of lysosomes in physiological activities, diseases, and therapy. *J. Hematol. Oncol.* **2021**, *14* (1), 79.

(21) Li, B. W.; Bai, Y.; Yion, C.; Wang, H.; Su, X.; Feng, G. Q.; Guo, M. M.; Peng, W. C.; Shen, B. X.; Zheng, B. Single-Atom Nanocatalytic Therapy for Suppression of Neuroinflammation by Inducing Autophagy of Abnormal Mitochondria. *ACS Nano* **2023**, *17* (8), 7511–7529.

(22) Li, B. W.; Yang, C. R.; Guo, M. M.; Wang, S. C.; Peng, W. C.; Guo, Q. L.; Ming, D.; Teng, Y.; Zheng, B. Ultrasound-Remote Selected Activation Mitophagy for Precise Treatment of Rheumatoid Arthritis by Two-Dimensional Piezoelectric Nanosheets. *ACS Nano* **2023**, *17* (1), 621–635.

(23) Zhai, Q. M.; Chen, X.; Fei, D. D.; Guo, X. Y.; He, X. N.; Zhao, W. M.; Shi, S. T.; Gooding, J. J.; Jin, F.; Jin, Y.; Li, B. Nanorepairers Rescue Inflammation-Induced Mitochondrial Dysfunction in Mesenchymal Stem Cells. *Adv. Sci.* **2022**, *9* (4), 2103839.

(24) Hu, M.; Luo, Q.; Alitongbieke, G.; Chong, S.; Xu, C.; Xie, L.; Chen, X.; Zhang, D.; Zhou, Y.; Wang, Z.; Ye, X.; Cai, L.; Zhang, F.; Chen, H.; Jiang, F.; Fang, H.; Yang, S.; Liu, J.; Diaz-Meco, M. T.; Su, Y.; Zhou, H.; Moscat, J.; Lin, X.; Zhang, X. K. Celastrol-Induced Nur77 Interaction with TRAF2 Alleviates Inflammation by Promoting Mitochondrial Ubiquitination and Autophagy. *Mol. Cell* **2017**, *66* (1), 141–153.

(25) Shirai, T.; Nakai, A.; Ando, E.; Fujimoto, J.; Leach, S.; Arimori, T.; Higo, D.; van Eerden, F. J.; Tulyeu, J.; Liu, Y. C.; Okuzaki, D.; Murayama, M. A.; Miyata, H.; Nunomura, K.; Lin, B.; Tani, A.; Kumanogoh, A.; Ikawa, M.; Wing, J. B.; Standley, D. M.; Takagi, J.; Suzuki, K. Celastrol suppresses humoral immune responses and autoimmunity by targeting the COMMD3/8 complex. *Sci. Immunol.* **2023**, *8* (81), No. eadc9324.

(26) Chen, X.; Zhao, Y.; Luo, W.; Chen, S.; Lin, F.; Zhang, X.; Fan, S.; Shen, X.; Wang, Y.; Liang, G. Celastrol induces ROS-mediated apoptosis via directly targeting peroxiredoxin-2 in gastric cancer cells. *Theranostics* **2020**, *10* (22), 10290–10308.

(27) Liu, X.; Zhao, P.; Wang, X.; Wang, L.; Zhu, Y.; Song, Y.; Gao, W. Celastrol mediates autophagy and apoptosis via the ROS/JNK and Akt/mTOR signaling pathways in glioma cells. *J. Exp. Clin. Cancer Res.* **2019**, *38* (1), 184.

(28) Yang, L.; Liu, X.; Yang, J.; Wang, K.; Ai, Z.; Shang, J.; Zhou, M. Biomimetic delivery of emodin via macrophage membrane-coated UiO-66-NH(2) nanoparticles for acute pancreatitis treatment. *Biochem. Biophys. Res. Commun.* **2024**, *702*, 149649.

(29) Zhang, Q.; Zhou, J.; Zhou, J.; Fang, R. H.; Gao, W.; Zhang, L. Lure-and-kill macrophage nanoparticles alleviate the severity of experimental acute pancreatitis. *Nat. Commun.* **2021**, *12* (1), 4136.

(30) Zhou, K.; Yang, C.; Shi, K.; Liu, Y.; Hu, D.; He, X.; Yang, Y.; Chu, B.; Peng, J.; Zhou, Z.; Qian, Z. Activated macrophage membrane-coated nanoparticles relieve osteoarthritis-induced synovitis and joint damage. *Biomaterials* **2023**, *295*, 122036.

(31) Yan, N.; Xu, J.; Liu, G.; Ma, C.; Bao, L.; Cong, Y.; Wang, Z.; Zhao, Y.; Xu, W.; Chen, C. Penetrating Macrophage-Based Nanoformulation for Periodontitis Treatment. *ACS Nano* **2022**, *16* (11), 18253–18265.



- (32) Xia, J. Y.; Wang, L. Y.; Shen, T. L.; Li, P.; Zhu, P. Y.; Xie, S. N.; Chen, Z. Y.; Zhou, F.; Zhang, J. F.; Ling, J.; Liu, X. R.; Yu, H.; Sun, J. H. Integrated manganese (III)-doped nanosystem for optimizing photothermal ablation: Amplifying hyperthermia-induced STING pathway and enhancing antitumor immunity. *Acta Biomater* **2023**, *155*, 601–617.
- (33) Wang, W. T.; Gao, Y. M.; Lin, Y.; Qian, Y. X.; Shen, J.; Zhou, N. L.; Tang, B. Z.; Zhang, M. Inflammatory Microenvironment-Responsive Nanomotors with NIR Photothermal Effect for Deep Inflammation Elimination and Infection Inhibition. *Adv. Funct. Mater.* **2024**, *35* (10), 2416684.
- (34) Lv, X. J.; Min, J.; Huang, J.; Wang, H. R.; Wei, S.; Huang, C. X.; Dai, J. F.; Chen, Z. R.; Zhou, H. T.; Xu, Y. Y.; Zhao, H.; Liu, Z.; Wang, J. Simultaneously Controlling Inflammation and Infection by Smart Nanomedicine Responding to the Inflammatory Microenvironment. *Adv. Sci.* **2024**, *11*, 39.
- (35) Zhou, Z. H.; Lan, H. B.; Tan, H. Y.; Wang, Y.; Chen, W.; Batur, S.; Fu, C. S.; Kong, L.; Yang, C. L.; Niu, B. N.; Guo, Y. Y.; Zhang, Z. P.; Huang, K. ROS-responsive biomimetic nanovesicles to plaque microenvironment in targeted therapy of atherosclerosis. *Nano Today* **2024**, *59*, 102530.
- (36) Sun, Y.; Ding, S. L.; Zhao, X. Y.; Sun, D. D.; Yang, Y. H.; Chen, M.; Zhu, C. L.; Jiang, B. Y.; Gu, Q.; Liu, H. Y.; Zhang, M. Z. Self-Reinforced MOF-Based Nanogel Alleviates Osteoarthritis by Long-Acting Drug Release. *Adv. Mater.* **2024**, *36*, 39.
- (37) Huang, J. L.; Hong, X. W.; Chen, S. X.; He, Y. C.; Xie, L. X.; Gao, F. L.; Zhu, C. H.; Jin, X.; Yan, H. H.; Ye, Y. X.; Shao, M. Y.; Du, X. R.; Feng, G. Z. Biomimetic Metal-Organic Framework Gated NanoplatforM for Sonodynamic Therapy against Extensively Drug Resistant Bacterial Lung Infection. *Adv. Sci.* **2024**, *11* (33), 2402473.
- (38) Zhao, J. L.; Cai, X. J.; Gao, W.; Zhang, L. L.; Zou, D. W.; Zheng, Y. Y.; Li, Z. S.; Chen, H. R. Prussian Blue Nanozyme with Multienzyme Activity Reduces Colitis in Mice. *Acs Appl. Mater. Inter* **2018**, *10* (31), 26108–26117.
- (39) Shi, Z. P.; Li, X. H.; Chen, J. F.; Dai, Z. D.; Zhu, Y. F.; Wu, T.; Liu, Q.; Qin, H. L.; Zhang, Y.; Chen, H. R. Enzyme-like biomimetic oral-agent enabling modulating gut microbiota and restoring redox homeostasis to treat inflammatory bowel disease. *Bioact Mater.* **2024**, *35*, 167–180.
- (40) Li, Z.; Fan, X. W.; Liu, Y.; Yue, M. X.; Wu, T. T.; Wang, X.; Jiang, W.; Fan, K. L. Engineering Mild-Photothermal Responsive and NO Donor Prussian Blue Nanozymes Using Mild Synthesis for Inflammation Regulation and Bacterial Eradication in Periodontal Disease. *Adv. Mater.* **2024**, *37* (6), 2409840.
- (41) Shen, K.; Li, X. W.; Huang, G. N.; Yuan, Z. W.; Xie, B.; Chen, T. F.; He, L. Z. High rapamycin-loaded hollow mesoporous Prussian blue nanozyme targets lesion area of spinal cord injury to recover locomotor function. *Biomaterials* **2023**, *303*, 122358.
- (42) Giorgio, M.; Trinei, M.; Migliaccio, E.; Pelicci, P. G. Hydrogen peroxide: a metabolic by-product or a common mediator of ageing signals? *Nat. Rev. Mol. Cell Biol.* **2007**, *8* (9), 722–728.
- (43) Slesak, I.; Slesak, H.; Zimak-Piekarczyk, P.; Rozpadek, P. Enzymatic Antioxidant Systems in Early Anaerobes: Theoretical Considerations. *Astrobiology* **2016**, *16* (5), 348–358.
- (44) Li, Q.; Wu, T. T.; Akakuru, O. U.; Song, N. N.; Liu, W.; Jiang, W.; Fan, K. L. A Dual Synergetic Nanoreactor for Managing Parkinson's Disease by Regulating Inflammation and Mitigating Oxidative Damage. *Adv. Funct. Mater.* **2023**, *33*, 37.
- (45) Voronina, S.; Chvanov, M.; De Faveri, F.; Mayer, U.; Wileman, T.; Criddle, D.; Tepikin, A. Autophagy, Acute Pancreatitis and the Metamorphoses of a Trypsinogen-Activating Organelle. *Cells* **2022**, *11*, 16.
- (46) Hu, M. J.; Luo, Q.; Alitongbieke, G.; Chong, S. Y.; Xu, C. T.; Xie, L.; Chen, X. H.; Zhang, D.; Zhou, Y. Q.; Wang, Z. K.; Ye, X. H.; Cai, L. J.; Zhang, F.; Chen, H. B.; Jiang, F. Q.; Fang, H.; Yang, S. J.; Liu, J.; Diaz-Meco, M. T.; Su, Y.; Zhou, H.; Moscat, J.; Lin, X. Z.; Zhang, X. K. Celastrol-Induced Nur77 Interaction with TRAF2 Alleviates Inflammation by Promoting Mitochondrial Ubiquitination and Autophagy. *Mol. Cell* **2017**, *66* (1), 141.
- (47) Gukovskaya, A. S.; Gukovsky, I.; Algül, H.; Habtezion, A. Autophagy, Inflammation, and Immune Dysfunction in the Pathogenesis of Pancreatitis. *Gastroenterology* **2017**, *153* (5), 1212–1226.
- (48) Li, J.; Yang, D.; Li, Z.; Zhao, M.; Wang, D.; Sun, Z.; Wen, P.; Dai, Y.; Gou, F.; Ji, Y.; Zhao, D.; Yang, L. PINK1/Parkin-mediated mitophagy in neurodegenerative diseases. *Ageing research reviews* **2023**, *84*, 101817.
- (49) Corson, T. W.; Crews, C. M. Molecular understanding and modern application of traditional medicines: Triumphs and trials. *Cell* **2007**, *130* (5), 769–774.
- (50) Guo, L.; Luo, S.; Du, Z. W.; Zhou, M. L.; Li, P. W.; Fu, Y.; Sun, X.; Huang, Y.; Zhang, Z. R. Targeted delivery of celastrol to mesangial cells is effective against mesangioproliferative glomerulonephritis. *Nat. Commun.* **2017**, *8*, 878.
- (51) Jiang, X. J.; Yuan, C. X.; Ding, R.; Lu, D.; Peng, X. Y.; Dong, Z. H.; Zhu, C. Y.; Lin, Y. H.; Wu, C. S.; Xie, Q. Toxic metabolites and metabolic soft spots of celastrol based on glutathione metabolic capture and high-resolution mass spectrometry. *Expert Opin. Drug Metab. Toxicol.* **2023**, *19* (12), 1023–1032.